

Radiation patterns for 2-D GPR forward modeling

José M. Carcione*

ABSTRACT

The electromagnetic (EM) radiation of a ground-penetrating radar (GPR) antenna is affected by the presence of the air-earth interface and depends on the geometrical and physical characteristics of the antenna. To simulate the radiation pattern with grid methods without the explicit modeling of these features, an equivalent solution is obtained by using a composite source concept. The 2-D analytic solution corresponding to magnetic and electric sources located at the same grid point is computed. This solution constitutes a basis for the construction of a composite source located in a small region of the numerical mesh.

The field is obtained for transverse magnetic (TM) and transverse electric (TE) waves in anisotropic media because the use of anisotropic conductivity is an alternative approach to simulating different radar apertures. Realistic radiation patterns are obtained from simple combinations of magnetic and electric sources by analogy with seismic shear stresses. The source parameterization is used for GPR simulation, and single radargram traces obtained with the modeling algorithm are cross checked with the analytic solution.

INTRODUCTION

The computation of realistic synthetic radargrams by grid methods (e.g., Greenfield and Wu, 1991; Kunz and Luebbers, 1993; Carcione, 1996) requires a proper simulation of the ground-penetrating radar (GPR) antenna radiation pattern. In principle, it is possible to obtain a precise numerical evaluation of the transient field radiation. For instance, Maloney et al. (1990) computed the directivity properties of simple antennas by using a finite-difference time-domain (FDTD) method. However, the explicit implementation of the antenna characteristics (geometry and material properties) for different heights relative to the ground, requires the use of a substantial region of the numerical mesh. For practical purposes, it is convenient to simulate the radiation pattern of the transmitting

antenna by an equivalent approach. If the directivity pattern of the antenna is known, either from a finite-difference simulation or an analytic evaluation (Annan, 1973; Arcone, 1995) or an experimental characterization (e.g., Wensink et al., 1990; Bernabini et al., 1995), it can then be simulated by a composite source concept.

The electromagnetic (EM) radiation produced by a composite source, located in a small region of the numerical mesh, can be obtained by summing the contributions of many single magnetic and electric sources. The superposition principle is valid because the EM equations used to compute the radargrams are linear. In addition, the composite source analysis provides an analytic solution for testing GPR simulation algorithms in anisotropic media. Note that anisotropy can be important in some cases (e.g., Tillard, 1994).

In the first section of this paper, I introduce the extended transverse magnetic (TM) radar equations for anisotropic media. Then, the solution to a single set of magnetic and electric sources is obtained. The third part provides the solution for a composite source using the superposition principle, and for completeness, the transverse electric (TE) solution is also given. Finally, the examples show the equivalence between earthquake and EM sources, the role of anisotropic conductivity in the radiation pattern, and the construction of realistic sources.

THE TM RADAR EQUATIONS

Assume that the propagation is in the (x, z) -plane, where x is horizontal position and z is depth, and that the material properties are constant along the y -coordinate. Then, the electric and magnetic field components E_x , E_z , and H_y are decoupled from E_y , H_x , and H_z . The first three fields obey the extended transverse magnetic (TM) differential equations (e.g., Harrington, 1961; Carcione, 1996):

$$\frac{\partial E_z}{\partial x} - \frac{\partial E_x}{\partial z} = \mu_0 \frac{\partial H_y}{\partial t} + M_y, \quad (1)$$

$$-\frac{\partial H_y}{\partial z} = \sigma_{11} * \frac{\partial E_x}{\partial t} + \epsilon_{11} * \frac{\partial^2 E_x}{\partial t^2} + J_x, \quad (2)$$

$$\frac{\partial H_y}{\partial x} = \sigma_{33} * \frac{\partial E_z}{\partial t} + \epsilon_{33} * \frac{\partial^2 E_z}{\partial t^2} + J_z, \quad (3)$$

Manuscript received by the Editor January 8, 1996; revised manuscript received April 3, 1997.

*Osservatorio Geofisico Sperimentale, P.O. Box 2011, Opicina, 34016, Trieste, Italy. E-mail: carcione@gems755.ogs.trieste.it.

© 1998 Society of Exploration Geophysicists. All rights reserved.

where μ_0 is the free-space magnetic permeability ($\mu_0 = 4\pi 10^{-7}$ H/m), ϵ_{11} and ϵ_{33} are the principal components of the permittivity relaxation tensor, and σ_{11} and σ_{33} are the principal components of the conductivity relaxation tensor. Moreover, J and M are the electric and magnetic current densities, respectively, and the symbol $*$ denotes time convolution.

The principal components are time-dependent and describe various relaxation processes of the material. For instance, in Carcione (1996) ϵ_{mm} , $m = 1$ or 3 , is a generalized Debye function that represents the different dielectric losses, and σ_{mm} is a Kelvin-Voigt relaxation function that models the out-of-phase component of the conduction current at high frequencies.

The TM equations (1), (2), and (3) can be transformed to the frequency domain and, after elimination of the electric field components, written in terms of the magnetic field as

$$\begin{aligned} & \beta_{33} \frac{\partial^2 \tilde{H}_y}{\partial x^2} + \beta_{11} \frac{\partial^2 \tilde{H}_y}{\partial z^2} + \mu_0 \omega^2 \tilde{H}_y \\ & = i\omega \tilde{M}_y + \beta_{33} \frac{\partial \tilde{J}_z}{\partial x} - \beta_{11} \frac{\partial \tilde{J}_x}{\partial z}, \end{aligned} \quad (4)$$

where a tilde denotes Fourier transform with respect to time. Coefficients β_{mm} , $m = 1, 3$ contain the information about the different permittivity and conductivity relaxation processes affecting the EM propagation. They are complex and frequency dependent and have form

$$\beta_{mm} = \left(\epsilon_{emm} - \frac{i}{\omega} \sigma_{emm} \right)^{-1} \quad m = 1, 3, \quad (5)$$

where ϵ_{emm} and σ_{emm} are the effective permittivity and conductivity components [they are real and frequency dependent, see Carcione (1996)]. Moreover, ω is the angular frequency and $i = \sqrt{-1}$. The effective permittivity and conductivity contribute to the EM wave velocity and dissipation, respectively. For clarity, we omit the subindex e in the subsequent analysis.

In some soils, the radar aperture is reduced by the presence of moisture. This effect, observed in the field (M. Pipan, Trieste University, personal communication), can be simulated by assuming that the conductivity is anisotropic. Although conductivity is a property of the medium, it is common in modeling to include near-source coupling effects as part of the effective source. Note that the conductivity in the source region can be anisotropic even in the case of propagation in an isotropic underground.

A plane-wave analysis of equations (1), (2), and (3), based on uniform waves, gives the following quality factor (Carcione, 1996),

$$Q = \frac{\text{Re}(\beta_{11}) + \text{Re}(\beta_{33}) \tan^2 \theta}{\text{Im}(\beta_{11}) + \text{Im}(\beta_{33}) \tan^2 \theta} \quad (6)$$

where θ is the angle between the z -axis and the propagation vector and Re and Im denote real and imaginary parts, respectively. Note that σ_{11} determines the attenuation in the z -direction and σ_{33} the attenuation in the x -direction.

EM FIELD OF A POINT SOURCE

The solution of equation (4) for homogeneous media was obtained by Carcione and Cavallini (1993, 1995) for the case $J_x = J_z = 0$. Here, the spatial derivatives in the electric currents imply the differentiation of the Green's function. Assume for

instance that the vertical electric current J_z is a delta function. Since the solution is the convolution of the Green's function with the source term, it can be obtained as the x spatial derivative of the Green's function. Thus, the solution to equation (4) is

$$\begin{aligned} \tilde{H}_y(r, \theta, \omega) & = \pi \omega \tilde{M}_y H_0^{(2)}(\alpha) + i\pi \mu_0 \omega^2 r \\ & \times (\sin \theta \tilde{J}_z - \cos \theta \tilde{J}_x) \alpha^{-1} H_1^{(2)}(\alpha), \end{aligned} \quad (7)$$

where $H_0^{(2)}$ and $H_1^{(2)}$ are Hankel functions of the second kind,

$$\alpha = \sqrt{\mu_0 \omega} r \left(\frac{\sin^2 \theta}{\beta_{33}} + \frac{\cos^2 \theta}{\beta_{11}} \right)^{1/2} \quad (8)$$

and

$$r = \sqrt{x^2 + z^2}. \quad (9)$$

In the derivation of equation (7), the property $(\partial/\partial\alpha)[H_0^{(2)}(\alpha)] = -H_1^{(2)}(\alpha)$ has been used. The time-domain solution is obtained by a numerical inverse Fourier transform.

SOLUTION AND RADIATION PATTERN OF A COMPOSITE SOURCE

Let us assume an EM source at a point of the form

$$\begin{aligned} \tilde{M}_y & = I_M \tilde{h}(\omega) \delta(x) \delta(z), & \tilde{J}_x & = I_x \tilde{h}(\omega) \delta(x) \delta(z), \\ \tilde{J}_z & = I_z \tilde{h}(\omega) \delta(x) \delta(z), \end{aligned} \quad (10)$$

where I_M , I_x , and I_z are the respective intensities, $\tilde{h}(\omega)$ is the source time Fourier transform, and δ denotes the Dirac function. Since $x = r \sin \theta$ and $z = r \cos \theta$, equation (7) can be rewritten as

$$\begin{aligned} \tilde{H}_y(x, z, \omega) & = \pi \omega [I_M H_0^{(2)}(\alpha) + i\mu_0 \omega (x I_z - z I_x) \\ & \times \alpha^{-1} H_1^{(2)}(\alpha)] \tilde{h}(\omega) \delta(x) \delta(z), \end{aligned} \quad (11)$$

with

$$\alpha = \sqrt{\mu_0 \omega} \left(\frac{x^2}{\beta_{33}} + \frac{z^2}{\beta_{11}} \right)^{1/2}. \quad (12)$$

A composite source can be obtained by summing the contributions of many single sources. Consider a composite source located in a rectangular region of the mesh where the material properties are homogeneous (see Figure 1). If the size of the rectangle is $2L_x \times 2L_z$ (measured in grid points) and the respective grid spacings are dx and dz , the total magnetic field can be expressed as

$$\begin{aligned} \tilde{H}_y(x, z, \omega) & = \pi \omega \sum_{i=-L_x}^{L_x} \sum_{j=-L_z}^{L_z} \{ I_M(i, j) H_0^{(2)}(\alpha_{ij}) \\ & + i\mu_0 \omega [(x - idx) I_z(i, j) - (z - jdz) I_x(i, j)] \\ & \times \alpha_{ij}^{-1} H_1^{(2)}(\alpha_{ij}) \} \tilde{h}(\omega) \delta(x - idx) \delta(z - jdz), \end{aligned} \quad (13)$$

where

$$\alpha_{ij} = \sqrt{\mu_0 \omega} \left[\frac{(x - idx)^2}{\beta_{33}} + \frac{(z - jdz)^2}{\beta_{11}} \right]^{1/2}. \quad (14)$$

As in the previous section, the time-domain magnetic field is obtained by a numerical inverse Fourier transform. The radiation pattern is a polar plot of the peak amplitude computed at the circle of radius r in a homogeneous medium, with $r \gg dx$ and $r \gg dz$.

SOLUTION FOR THE TE MODE

For completeness, the solution for the transverse electric (TE) mode is presented in this section. The TE equations are

$$\frac{\partial E_y}{\partial z} = \mu_0 \frac{\partial H_x}{\partial t} + M_x, \quad (15)$$

$$-\frac{\partial E_y}{\partial x} = \mu_0 \frac{\partial H_z}{\partial t} + M_z, \quad (16)$$

$$\frac{\partial H_x}{\partial z} - \frac{\partial H_z}{\partial x} = \sigma_{22} * \frac{\partial E_y}{\partial t} + \epsilon_{22} * \frac{\partial^2 E_y}{\partial t^2} + J_y, \quad (17)$$

where ϵ_{22} and σ_{22} are the principal components of the permittivity and conductivity relaxation tensor. A transformation to the frequency-domain yields for the electric field

$$\frac{\partial^2 \tilde{E}_y}{\partial x^2} + \frac{\partial^2 \tilde{E}_y}{\partial z^2} + \frac{\mu_0}{\beta_{22}} \omega^2 \tilde{E}_y = i\omega\mu_0 \tilde{J}_y - \frac{\partial \tilde{M}_z}{\partial x} + \frac{\partial \tilde{M}_x}{\partial z}. \quad (18)$$

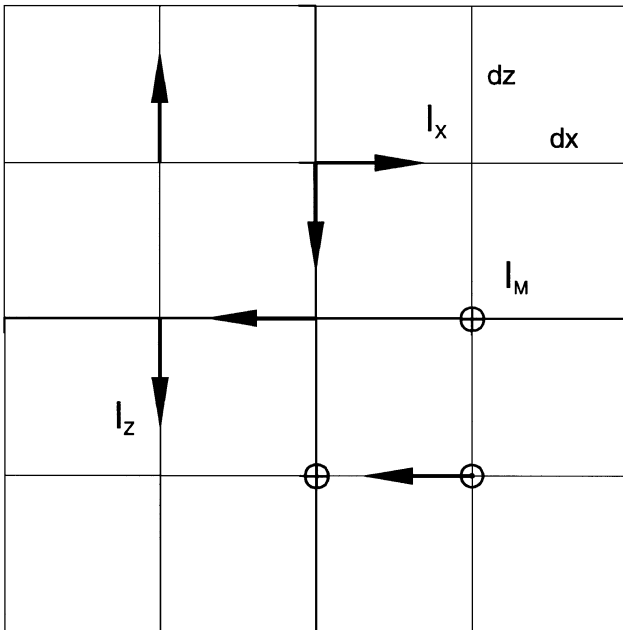


FIG. 1. Illustration of the composite source concept. The contribution of many single magnetic and electric sources located in a small region of the numerical mesh gives a composite source with a general directivity pattern. The grid spacings are denoted by dx and dz ; I_x and I_z are the intensities of the electric sources, and I_M is the intensity of the magnetic source at each grid point. For instance, if all the grid points illustrated in the figure are used to construct the composite sources, the numbers of free parameters to fit a given radiation pattern is $25 \times 3 = 75$.

The TE solution for a single source is obtained from equations (7), (8), and (9) by making the following substitutions:

TM	TE
H_y	$\rightarrow E_y$
β_{11}	$\rightarrow \beta_{22}$
β_{33}	$\rightarrow \beta_{22}$
M_y	$\rightarrow \mu_0 \beta_{22} \tilde{M}_y$
\tilde{J}_z	$\rightarrow -\tilde{M}_z$
\tilde{J}_x	$\rightarrow -\tilde{M}_x$.

Substituting these into equation (13) gives the composite TE source solution.

EXAMPLES

The EM field obtained from the analytic solution (13) is used to calculate radiation patterns, i.e., the source intensities I_M , I_x , and I_z in a given region of the numerical mesh. Then, the radar equations are solved with a direct grid method that computes the spatial derivatives by using the Fourier pseudospectral method and propagates the solution in time with an explicit fourth-order Runge-Kutta algorithm (Carcione and Cavallini, 1994; Carcione, 1996). The snapshots presented in the following figures are computed with this simulation method.

The calculations assume the source time function

$$h(t) = \exp[-2f_c^2(t - t_0)^2] \cos 2\pi f_c(t - t_0), \quad (19)$$

whose Fourier transform is

$$\tilde{h}(\omega) = \frac{\sqrt{2\pi}}{f_c} \exp(i\omega t_0) \left\{ \exp\left[-2\pi^2 \left(\frac{1}{2} - \frac{\omega}{\pi f_c}\right)^2\right] + \exp\left[-2\pi^2 \left(\frac{1}{2} + \frac{\omega}{\pi f_c}\right)^2\right] \right\}, \quad (20)$$

where f_c is the central frequency and $t_0 = 3/(2f_c)$ is a time delay.

Consider a medium with $\epsilon_{11} = \epsilon_{33} = 25\epsilon_0$ ($\epsilon_0 = 8.85 \times 10^{-12}$ F/m) and $\sigma_{11} = 0$. Figure 2 displays two snapshots of the magnetic field at 50 ns for a source with a central frequency of 200 MHz. The snapshots correspond to a single magnetic source located at the center of a 3×3 m region and a grid spacing of $dx = dz = 7.5$ cm. In (a), the medium is lossless ($\sigma_{33} = 0$), implying an isotropic amplitude distribution. In (b), $\sigma_{33} = 0.01$ S/m, and the radiation pattern is anisotropic. A polar representation of the quality factor (6) corresponding to Figure 2b is shown in Figure 3a, indicating that the medium is lossless only in the vertical direction [$Q(\theta = 0) \rightarrow \infty$].

The normalized radiation pattern in the lossless medium, at a radial distance of 1.5 m, is represented in Figure 3b. As can be seen, the amplitude distribution is isotropic. The effect of the anisotropic conductivity depends on the distance from the source: the radiation patterns at 1.5 m and 3 m from the source are represented in Figures 3c and 3d, respectively. In this way, different radar apertures can be simulated.

Carcione and Cavallini (1995) investigated the analogy between EM and shear-wave propagation. They showed that the

propagation of the TM mode is governed by the same differential equations describing antiplane shear-wave motion. A consequence of this mathematical analogy is that the EM radiation patterns are equivalent to shear directivity patterns. In fact, the following sources yield the typical seismic wave radiation patterns (e.g., Pilant, 1979, 352):

$$\begin{aligned} I_z(0, 0) &= 1, & \text{vertical electric current} \\ I_z(-1, 0) &= -1, \quad I_z(1, 0) = 1, & \text{couple with moment} \\ I_z(0, -1) &= -1, \quad I_z(0, 1) = 1, & \text{linear doublet} \\ I_x(0, 1) &= 1, \quad I_x(0, -1) = -1 \\ I_z(-1, 0) &= -1, \quad I_z(1, 0) = 1, & \text{double couple with moment.} \end{aligned}$$

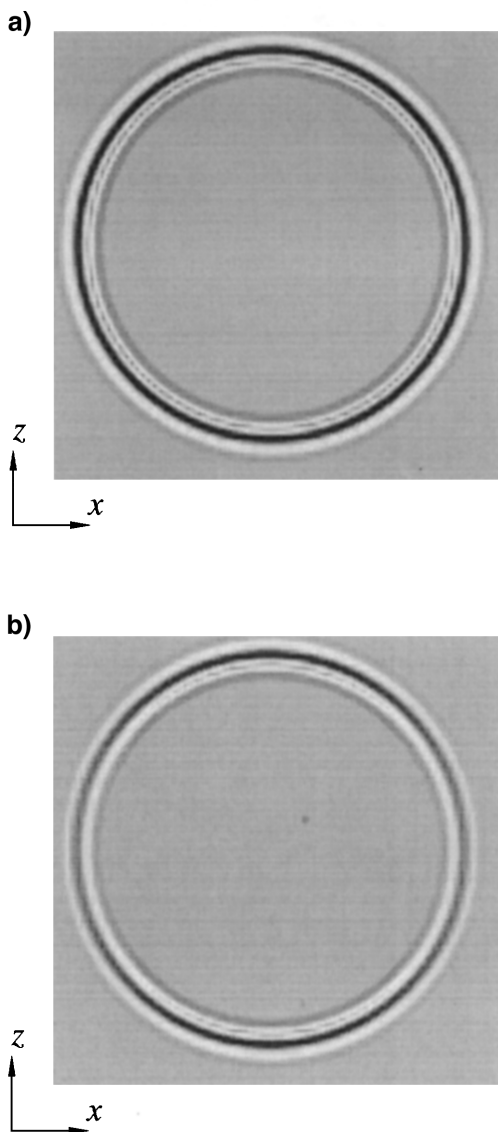


FIG. 2. Snapshots of the magnetic field at 50 ns corresponding to a single magnetic source of 200 MHz central frequency. The size of the model is 3×3 m. In (a), the medium is lossless; in (b), $\sigma_{11} = 0$ and $\sigma_{33} = 0.01$ S/m.

The magnetic dipole $I_M(0, -1) = -1$, $I_M(0, 1) = 1$ gives the snapshot and radiation pattern shown in Figures 4a and 4b, respectively. Measurements of the radiation pattern of a dipole bistatic GPR antenna in air by Bernabini et al. (1995) are represented by dots in Figure 5b. An equivalent source is obtained by matching the experimental points with the inverse Fourier transform of equation (13), using the intensities I_M , I_x , and I_z as fitting parameters. A standard nonlinear curve-fitting algorithm is used to obtain the following composite source:

$$\begin{aligned} I_x(0, -1) &= 0.4 \text{ A}, & I_x(1, 1) &= 0.3 \text{ A}, \\ I_x(0, 0) &= -10 \text{ A}, & I_x(-1, -1) &= -0.1 \text{ A}, \\ I_x(0, -1) &= 1.2 \text{ A}, & I_x(1, -1) &= 0.5 \text{ A}, \\ I_M(-1, 1) &= -0.25 \gamma \text{ A}, & I_M(0, 1) &= 0.15 \gamma \text{ A}, \\ I_M(1, 1) &= -0.02 \gamma \text{ A}, & I_M(-1, 0) &= -0.15 \gamma \text{ A}, \\ I_M(0, 0) &= 2.3 \gamma \text{ A}, & I_M(1, 0) &= -0.14 \gamma \text{ A}, \\ I_M(-1, -1) &= -0.12 \gamma \text{ A}, & I_M(0, -1) &= 0.1 \gamma \text{ A}, \\ I_M(1, -1) &= 0.18 \gamma \text{ A}, \end{aligned}$$

where $\gamma = (\mu_0/\epsilon_0)^{1/2}$. Figure 5e illustrates a radargram corresponding to a test model whose background medium has permittivity of $25 \epsilon_0$ and the rectangular objects have a permittivity of $4 \epsilon_0$. The antenna is located above the center object and has a frequency of 200 MHz (the earth's surface is not modeled). A numerical mesh of 225×81 is used, with a grid spacing of 7.5 cm in the vertical and horizontal directions. The center object produces the strongest reflection, since most of the energy is directed downward.

Finally, Figure 6 compares analytic and numerical solutions (continuous line and dots, respectively) of the magnetic field along three different directions at $r = 1.5$ m, corresponding to the following source:

$$I_x(0, -1) = 1 \text{ A}, \quad I_x(0, 1) = -1 \text{ A}, \quad I_M(0, 1) = 0.2 \gamma \text{ A}.$$

The solutions are normalized with respect to the receiver located at 180° . As can be seen, the agreement is virtually perfect, giving a cross check of both analytic and modeling solutions.

CONCLUSIONS

The composite source concept provides a method to simulate arbitrary radiation patterns from GPR antennas and to save computer memory and time by reducing the amount of grid points used for modeling the antenna. The method simulates the far field radiated energy with, in general, no more than nine grid points, i.e., a 3×3 region of the numerical mesh. The use of an anisotropic medium at the source location allows flexible control of the directivity properties. It is shown how anisotropic conductivity affects the radar aperture.

Simple sources can be used as a base to construct complex directivity patterns that simulate the radiation of a complex antenna configuration in homogeneous media and in the presence of the air-earth interface. Moreover, the analysis gives the solution of a complex distribution of sources in a medium with

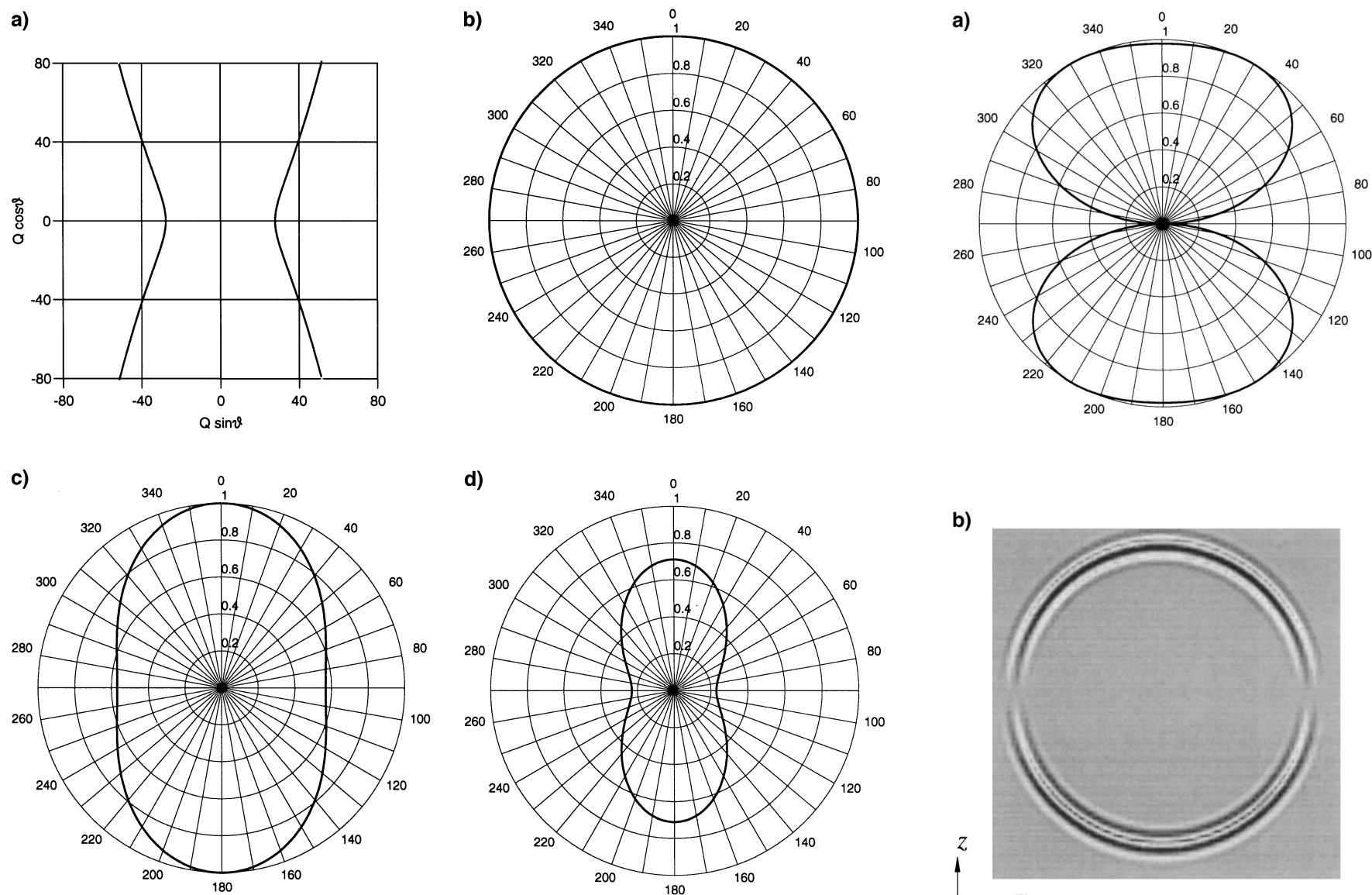


FIG. 3. (a) A polar representation of the quality factor corresponding to the medium whose snapshots are shown in Figure 2b; (b) normalized radiation pattern in a lossless and isotropic medium; (c) and (d) are radiation patterns in a lossy medium (as in Figure 2b) at distances of 1.5 m and 3 m, respectively, from the source.

FIG. 4. Radiation pattern (a) and snapshot (b) corresponding to a magnetic dipole.

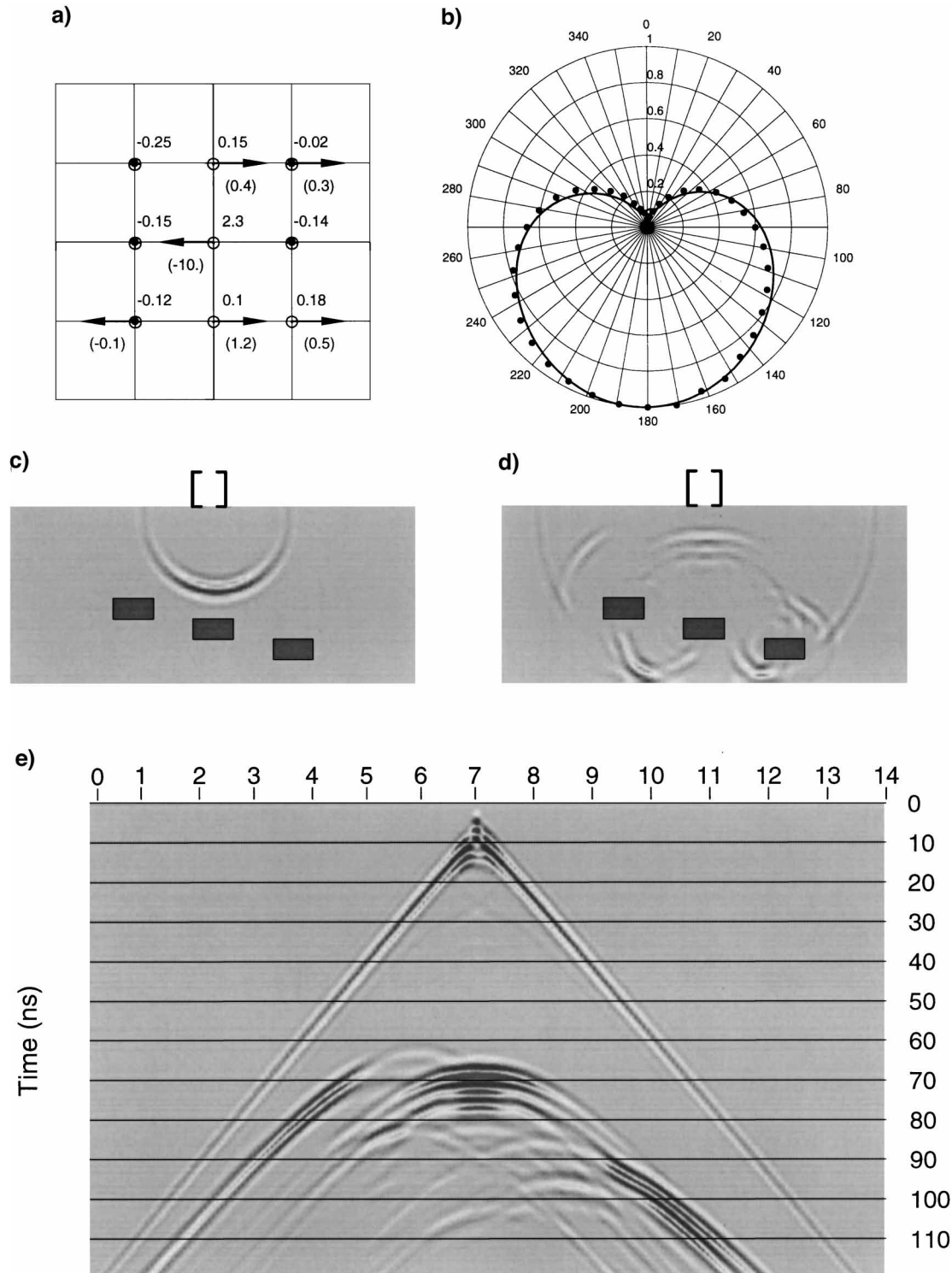


FIG. 5. Source distribution (a), radiation pattern (b), snapshots [at 30 ns (c) and 60 ns (d)], and radargram (e), corresponding to a real antenna, whose experimental values (measured by Bernabini et al., 1995), are indicated by dots. The background medium of the test model has a permittivity of $25 \epsilon_0$ and the rectangular objects (0.75 m width) have a permittivity of $4 \epsilon_0$. The numbers in (a) indicate the values of the magnetic intensities (in γA) and of the electric intensities (in parentheses, in A).

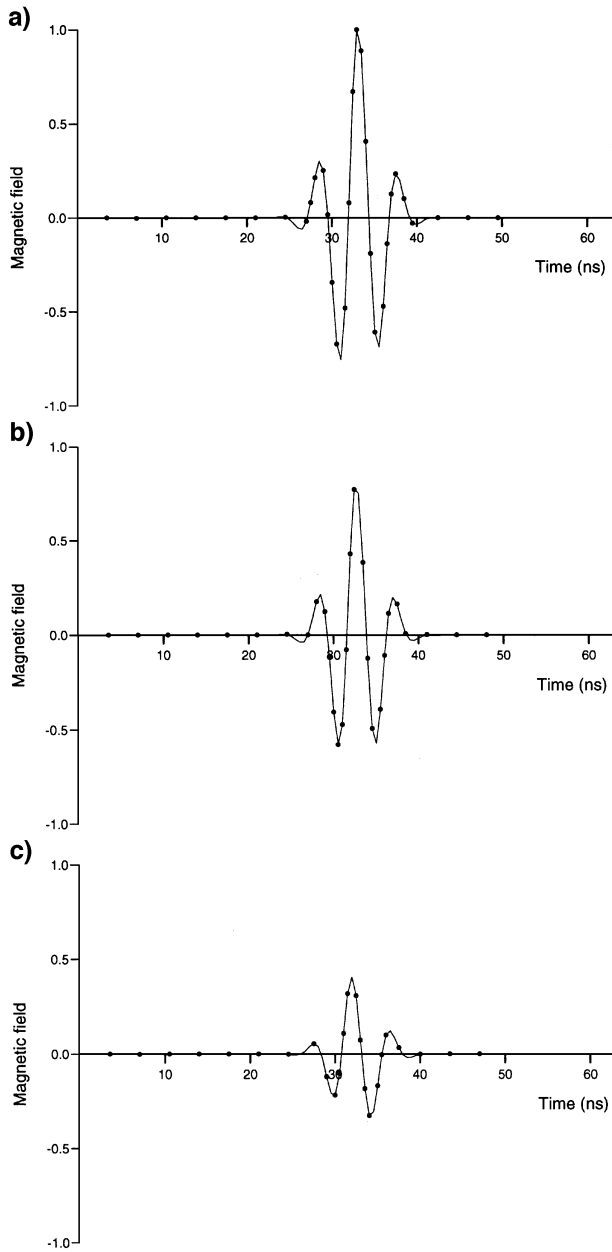


FIG. 6. Comparison between analytic (solid line) and numerical (dots) solutions at (a) 180° , (b) 135° , and (c) 90° for a composite source.

anisotropic permittivity and conductivity properties and general frequency-domain behaviour. This solution can be used to test GPR forward modeling codes based on grid methods.

The research may proceed as follows. The simulation of composite pulses could be obtained by initiating sources at different times and positions in the radiation process, or using as fitting parameters the whole source time history instead of the maximum intensities. In addition, anisotropic permittivity can be used to model a nonisotropic wavefront arising from an arbitrary antenna shape. The concept can be easily extended to the three-dimensional case, provided that the 3-D Green's function for single magnetic and electric sources can be obtained in closed analytic form.

ACKNOWLEDGMENT

This work was funded in part by AGIP S.p.A.

REFERENCES

- Annan, A. P., 1973, Radio interferometry depth sounding: Part I— theoretical discussion: *Geophysics*, **38**, 557–580.
- Arcone, S. A., 1995, Numerical studies of the radiation patterns of resistivity loaded dipoles, *J. Appl. Geophys.*, **33**, 39–52.
- Bernabini, M., Pettinelli, E., Pierdicca, N., Piro, S., and Versino, L., 1995, Field experiments for characterization of GPR antenna and pulse propagation: *J. Appl. Geophys.*, **33**, 63–76.
- Carcione, J. M., 1996, Ground penetrating radar: wave theory and numerical simulation in lossy anisotropic media: *Geophysics*, **61**, 1664–1677.
- Carcione, J. M., and Cavallini, F., 1994, Modeling transverse electromagnetic waves in conducting anisotropic media by a spectral time-domain technique, *in* Terzuoli, A., Ed., 10th Annual Review of Progress in Applied Computational Electromagnetics, Vol. II, 586–593.
- 1993, A semi-analytical solution for the propagation of pure shear waves in dissipative monoclinic media: *Acoust. Lett.*, **17**, 72–76.
- 1995, On the acoustic-electromagnetic analogy: *Wave Motion*, **21**, 149–162.
- Greenfield, R. J., and Wu, T., 1991, Electromagnetic wave propagation in disrupted coal seams: *Geophysics*, **56**, 1571–1577.
- Harrington, R. F., 1961, *Time-harmonic electromagnetic fields*; Mc-Graw Hill Book Co.
- Kunz, K. S., and Luebbers, R. J., 1993, *The finite-difference time domain method for electromagnetics*, CRC Press.
- Maloney, J. G., Smith, G. S., and Scott, Jr., W. R., 1990, Accurate computation of the radiation from simple antennas using the finite-difference time-domain method: *IEEE Trans. Antennas Propagat.*, **38**, 1059–1068.
- Pilant, W. L., 1979, *Elastic waves in the earth*; Elsevier Publ. Co.
- Tillard, S., 1994, Radar experiments in isotropic and anisotropic geological formations (granite and schists): *Geophys. Prosp.*, **42**, 615–636.
- Wensink, W. A., Greeuw, G., Hofman, J., and Van Deen, J. K., 1990, Measured underwater near-field E-patterns of a pulsed, horizontal dipole antenna in air: Comparison with the theory of the continuous wave, infinitesimal electric dipole: *Geophys. Prosp.*, **38**, 805–830.